Magnetic Resonance in Medicine 58:354–364 (2007)

Fat Quantification With IDEAL Gradient Echo Imaging: Correction of Bias From T_1 and Noise

Chia-Ying Liu,[1,2*] Charles A. McKenzie,[5] Huanzhou Yu,[6] Jean H. Brittain,[7] and Scott B. Reeder[1–4]

Quantification of hepatic steatosis is a significant unmet need for the diagnosis and treatment of patients with nonalcoholic fatty liver disease (NAFLD). MRI is capable of separating water and fat signals in order to quantify fatty infiltration of the liver (hepatic steatosis). Unfortunately, fat signal has confounding T_1 effects and the nonzero mean noise in low signal-to-noise ratio (SNR) magnitude images can lead to incorrect estimation of the true lipid percentage. In this study, the effects of bias from T_1 effects and image noise were investigated. An oil/water phantom with volume fat-fractions ranging linearly from 0% to 100% was designed and validated using a spoiled gradient echo (SPGR) sequence in combination with a chemical-shift based fat-water separation method known as iterative decomposition of water and fat with echo asymmetry and least squares estimation (IDEAL). We demonstrated two approaches to reduce the effects of T_1: small flip angle (flip angle) and dual flip angle methods. Both methods were shown to effectively minimize deviation of the measured fat-fraction from its true value. We also demonstrated two methods to reduce noise bias: magnitude discrimination and phase-constrained reconstruction. Both methods were shown to reduce this noise bias effectively from 15% to less than 1%. Magn Reson Med 58:354–364, 2007. © 2007 Wiley-Liss, Inc.

Key words: fat quantification; IDEAL; chemical shift imaging; hepatic steatosis; magnetic resonance imaging

The importance of fatty infiltration (hepatic steatosis) in the progression of diffuse liver disorders is well documented (1–4). Nonalcoholic fatty liver disease (NAFLD) is a condition with increasing recognition as the most common cause of chronic liver disease, afflicting an estimated 14% to 30% of the general population (2,5) in the United States. NAFLD is closely linked with insulin resistance and is thought by many to be the hepatic manifestation of the "metabolic syndrome." In an important subset of patients with NAFLD, steatosis progresses to inflammation and fibrosis, a condition known as nonalcoholic steatohepatitis (NASH). Up to 3% of all Americans may be afflicted with NASH; of these, 27% progress to end-stage cirrhosis and 12% die of liver failure (4,6,7).

The earliest manifestation and hallmark of NAFLD/NASH is steatosis. However, accurate and early diagnosis of steatosis is difficult because its assessment relies on liver biopsy (8,9). Unfortunately, the utility of biopsy, the current gold standard, is very limited. Steatosis can have a heterogeneous distribution, and nontargeted liver biopsy has very high sampling variability (8). In addition, histological evaluations of steatosis are graded on a subjective scale. A distinct disadvantage of liver biopsy is that it is an invasive procedure with a risk of morbidity or mortality. Rates of complication vary with procedures, ranging from 1.3% to 20.2%, approximately 1% to 3% of patients require hospitalization (9). Quantitative assessment of hepatic steatosis using noninvasive imaging techniques is highly desirable for the diagnosis and evaluation of fatty liver disease. Such a method could be performed frequently to track the evolution of steatosis in clinical trials for the evaluation of new drugs in the treatment of hepatic steatosis (10,11). Accurate quantification of steatosis could also enhance the statistical power of drug trials, greatly reducing the number of patients needed to determine drug therapy effectiveness.

Preliminary MRI using chemical shift based techniques (12–16) to generate in-phase and out-of-phase images has been clinically studied for quantification of liver fat content (17–19). However, this approach suffers from a natural ambiguity; as noted by Hussein et al. (19), fat-fractions greater than 50% cannot be distinguished easily from fat-fractions less than 50%; for example, a fat-fraction of 30% causes the same signal dropout as a 70% fat-fraction. It is difficult to determine fat-fraction over a range of 0% to 100% unless the water and fat signals are fully separated. Unfortunately, true separation of water and fat with in/out phase imaging is highly sensitive to magnetic field inhomogeneities (12), and requires more advanced imaging and reconstruction methods (13–16).

Regardless of the fat-water separation imaging technique, different relaxation times between water and fat result in a significant bias in the estimate of fat-fraction. This occurs because the shorter T_1 of fat causes a relative signal amplification of fat compared to water. For example, the T_1 of fat and water in the liver at 1.5T are approximately 343 ms and 586 ms, respectively (20). Consequently, true fat-fraction images cannot be obtained in the presence of T_1 weighting. The effect of T_2* must also be considered in diseased livers with iron overload, even though it can be ignored in normal livers for short-TE

[1]Department of Radiology, University of Wisconsin-Madison, Madison, WI, USA.
[2]Department of Medical Physics, University of Wisconsin-Madison, Madison, WI, USA.
[3]Department of Biomedical Engineering, University of Wisconsin-Madison, Madison, WI, USA.
[4]Department of Medicine, University of Wisconsin-Madison, Madison, WI, USA.
[5]Department of Radiology, Beth Israel-Deaconess Medical Center and Harvard Medical School, Boston, MA, USA.
[6]Global Applied Science Laboratory, GE Healthcare, Menlo Park, CA, USA.
[7]Global Applied Science Laboratory, GE Healthcare, Madison, WI, USA.

Grant sponsors: University of Wisconsin (UW) System Applied Research Grant.

*Correspondence to: Chia-Ying Liu, Ph.D., Department of Radiology, J5/M150, CSC, University of Wisconsin, 600 Highland Avenue, Madison, WI 53792-3252. E-mail: cliu25@wisc.edu

Received 9 December 2006; Revised 21 March 2007; Accepted 18 April 2007.
DOI 10.1002/mrm.21301
Published online in Wiley InterScience (www.interscience.wiley.com).

gradient echo imaging. Although we have demonstrated the ability to correct for shortened T_2* (21), for the purposes of this work, we will ignore the effects of T_2*, and report T_2* compensation methods in hepatic iron overload elsewhere.

In addition to the relaxation effects, the influence of image noise must also be considered. For most fat-water separation methods, which use complex images to separate water and fat, the subsequent calculation of fat-fraction is based on magnitude fat and water images. Noise bias is introduced in areas with low signal due to the skewed noise distribution from the magnitude operation. This effect will have great clinical importance in low fat content regions affecting the diagnosis of mild steatosis.

A multipoint chemical-shift–based fat-water decomposition technique known as iterative decomposition of water and fat with echo asymmetry and least squares estimation (IDEAL) (16,22,23) has been shown to be a robust method for separation of water and fat signals. IDEAL uses asymmetric phase shifts ($\theta = -\pi/6+\pi k, \pi/2+\pi k, 7\pi/6+\pi k$, k = integer, echo times [TE] = $\theta/(2\pi\Delta f)$, where Δf is the chemical shift between fat and water, which is approximately −210 Hz at 1.5T and −420 Hz at 3.0T), to improve the effective number of signal averages (NSA) noise performance to the maximum possible value of 3 over the entire range of fat-water proportions (16,22,24). NSA is equivalent to the signal-to-noise ratio (SNR) of three averaged images and can be used to describe the noise performance in the fat-water separation algorithm (13,16). The largest obstacle to volumetric quantification of hepatic fat content with MRI is the need to acquire all the necessary data within one reasonable breath-hold duration to avoid movement artifacts, which corresponds to ~30 s in the young and healthy population, but perhaps significantly less in the disease population. Spoiled gradient recalled echo (SPGR) is a commonly used sequence for three-dimensional (3D) volumetric liver imaging. IDEAL has been combined with parallel imaging (25) and incorporated with multiecho SPGR sequence (26) to further accelerate scan time, permitting image acquisition over the whole liver in a short breathhold. The multiecho SPGR sequence in combination with the IDEAL reconstruction provides breathheld acquisitions over the entire liver and reliable fat-water separated images, and is therefore an excellent choice for accurate fat quantification.

The purpose of our study was to investigate the effects of T_1 and noise bias on fat quantification and to propose solutions to avoid these biases. We first describe the sources of these biases, potential solutions for correction, and then demonstrate the effectiveness of the proposed algorithm with IDEAL-SPGR water-fat separation methods. Quantitative analysis using a fat/water phantom was performed for evaluation of the small flip angle and dual flip angle approaches to reduce T_1 bias. The bias created by image noise was studied using a water phantom and methods including magnitude discrimination and phase-constrained approaches were examined.

THEORY

Definition of Fat-Fraction

Triglycerides are the primary component of accumulated lipids, all of which is contained within intracellular vacuoles of hepatocytes in steatotic livers (27). The NMR spectrum of intracellular lipid consists of multiple fatty acid peaks including olefinic (-CH = CH-), methylene (-$(CH_2)_n$-), and methyl (-CH_3) protons (28,29). Olefinic protons are unsaturated lipids and have a chemical shift of 5.35 ppm, which is close to that of water (4.65 ppm). Therefore, signal from olefinic protons will contribute to water images in chemical shift imaging methods. However, only the signals from methylene (1.3 ppm) and methyl (0.9 ppm) protons are of clinical significance in diagnosis of hepatic steatosis, directly reflecting the concentration of fatty acids that accumulate in patients with insulin resistance. Accordingly we define true fat-fraction as,

$$\eta = \frac{M_f}{(M_w + M_f)}, \quad [1]$$

where M_w and M_f are water and fat (-CH_2- and -CH_3 groups only) proton densities respectively. In MRI, we measure water and fat signal intensities to represent their proton densities (ignoring relaxation effects). Hence, the apparent (or signal) fat-fraction can be defined according to

$$\eta_s = \frac{S_f}{(S_w + S_f)}. \quad [2]$$

In Eq. [2], the water (S_w) signal includes contributions from olefinic protons and fat (S_f) signal contains only methylene and methyl groups. Using this definition, the fat-fraction is reflected accurately and provides a useful scale between 0% and 100%. System effects such as coil sensitivity are normalized out through the use of the fat-fraction, providing system independent results.

If the percentage of signal from the olefinic protons relative to the total fat, κ, is known, the fat-fraction can be easily corrected as

$$\hat{\eta}_s = \frac{S_f}{(S_w + S_f(1 - \kappa))}. \quad [3]$$

For example, consider $\eta_s = 0.5$ and $\kappa = 10\%$ (a reasonable assumption according to Yeung et al. (29)). Without the correction from Eq. [3], there will be a 2.6% decrease of the apparent fat-fraction, a relatively small error, for this "worst-case" scenario. For the purposes of describing the effects of T_1 and noise bias in this work, the effects of the olefinic peaks will be ignored.

Although the definition we described above represents the true proton density fat-fraction, it may not correspond to the volume fraction of lipids within a voxel due to small differences between the proton densities of triglycerides and water. We believe that the proton density fraction of fat may be a more meaningful and practical definition, since it is a measure that is independent of relaxation parameters (T_1, T_2*), and is therefore independent of pulse sequence acquisition parameters.

Confounding T_1 Effects on Fat-Fraction

The water signal S_w for SPGR depends on T_{1w}, T_{2w}*, α, the repetition time (TR), the echo time (TE), and the proton density M_w as given by Eqs. [4] and [5] (for fat) (30,31),

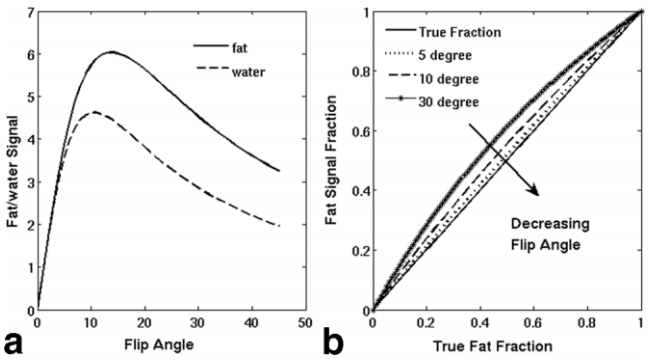

FIG. 1. **a:** Simulated fat and water signal behavior vs. flip angles using SPGR sequence with TR = 10 ms, T_{1w} = 586 ms, and T_{1f} = 343 ms and assuming the same fat/water proton densities. **b:** Simulated fat-fraction of various flip angles. The deviation of the signal fraction from the true value decreases with decreasing flip angle. A maximum error of 23% was calculated with a 30° flip angle, while there is only 4% error with a 5° flip angle, at equal amounts of fat and water.

$$S_w = \frac{M_w(1 - e^{-TR/T_{1w}})e^{-TE/T_{2w}^*}\sin\alpha}{(1 - e^{-TR/T_{1W}}\cos\alpha)} \quad [4]$$

$$S_f = \frac{M_f(1 - e^{-TR/T_{1f}})e^{-TE/T_{2f}^*}\sin\alpha}{(1 - e^{-TR/T_{1f}}\cos\alpha)} \quad [5]$$

In fast imaging techniques, TE is relatively short compared to the T_2* of the species in question (TE ≈ 4–7 ms and T_2* ≈ 26 ms in normal liver (32)). For the purpose of this work, T_2* effects can be ignored, although in patients with concomitant iron overload and steatosis, T_2* may become important and can be incorporated into the IDEAL signal model (21). The fat signal fraction η_s, which depends on S_w and S_f, will also depend on flip angle when the T_1 values of fat and water are unequal. This implies that η_s will be different from the true fat-fraction, η, as described by Eqs. [1] and [2].

The simulated fat/water signal behavior (assuming $M_w = M_f$, in Fig. 1a) and fat signal fractions (Fig. 1b) for a given TR = 10 ms, T_{1f} = 343 ms, and T_{1w} = 586 ms at 1.5T (20) of various flip angles demonstrate this effect, which the larger the flip angle, the more deviation of the fat-fraction from its true value.

Figure 2 demonstrates 3D IDEAL-SPGR fat-signal fraction images acquired in a patient with known steatosis. Fat-fraction from the same region of interest varies significantly (29–45%) with flip angle (5°–30°) due to T_1 effects as discussed above. Without T_1 correction, this error will lead to severe inaccuracy in the diagnosis of hepatic steatosis.

Small Flip Angle Approach

The proton densities can be calculated correctly if the T_1 of both water and fat are known. The measured signal intensity (S_w, S_f), and the known flip angle α, allows M_w and M_f to be calculated as follows,

$$M_w = \frac{S_w(1 - e^{-TR/T_{1w}}\cos\alpha)}{(1 - e^{-TR/T_{1w}})\sin\alpha} \quad [6]$$

$$M_f = \frac{S_f(1 - e^{-TR/T_{1f}}\cos\alpha)}{(1 - e^{-TR/T_{1f}})\sin\alpha}. \quad [7]$$

However, T_1 values are unknown in general and may vary in different disease states, particularly in the presence of iron or copper deposition (33,34). T_1 mapping is not part of routine clinical assessment owing to the lengthy scan times associated with the T_1 measurements (35). To reduce the influence of the T_1 dependence of the SPGR sequence on fat quantification, a small flip angle may be used. This is due to the first order Taylor expansion with respect to small α in Eq. [4], i.e., $\cos\alpha \approx 1$, $\sin\alpha \approx \alpha$ which simplifies the signal relation to $S_w \approx M_w\alpha$. Hence the flip angle term cancels in the fat-fraction calculation and the two definitions in Eqs. [1] and [2] are equal:

$$\eta_s = \frac{S_f}{(S_w + S_f)} \approx \frac{M_f\alpha}{(M_w\alpha + M_f\alpha)} = \frac{M_f}{(M_w + M_f)} = \eta. \quad [8]$$

SNR performance must be considered when small flip angles are used because SNR of an SPGR acquisition decreases rapidly at small flip angles (Fig. 1a). For example, using a flip angle of 5° will reduce the signal by 46% and 33% from the maximum amplitudes of fat and water, respectively. Figure 3a shows the results of a Monte Carlo simulation (3000 trials) that plots the SD of the fat-fraction (noise) caused by the addition of zero-mean Gaussian noise added to both the water and fat signals. For a specified SNR value, the SD of the noise was determined by measuring the signal from water at the Ernst angle (S^W_{Ernst}), with T_1^W = 586 ms, TR = 10 ms, α_{Ernst} = 11°, ie: $\sigma = SNR/S^W_{Ernst}$. For all simulations in Fig. 3a, the true fat-fraction is fixed at 0.5, and the SD on the fat-fraction was calculated from the 3000 trials to estimate the noise

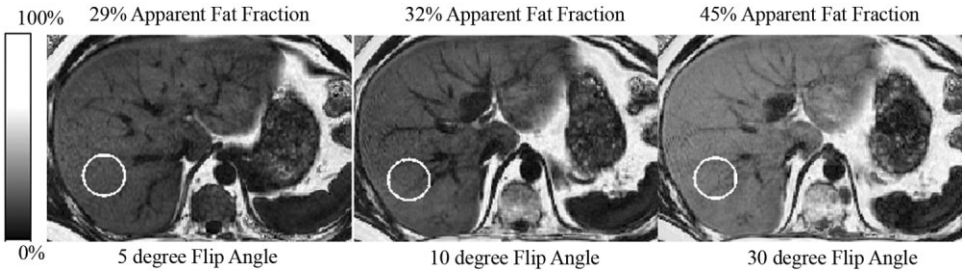

FIG. 2. Fat-signal fraction images acquired with 3D IDEAL-SPGR in a patient with known steatosis. Apparent fat-fraction from the same region of interest varies (29–45%) with flip angle (5° to 30°) used in imaging acquisitions. This large bias is due to difference in T_1 between water and fat signals.

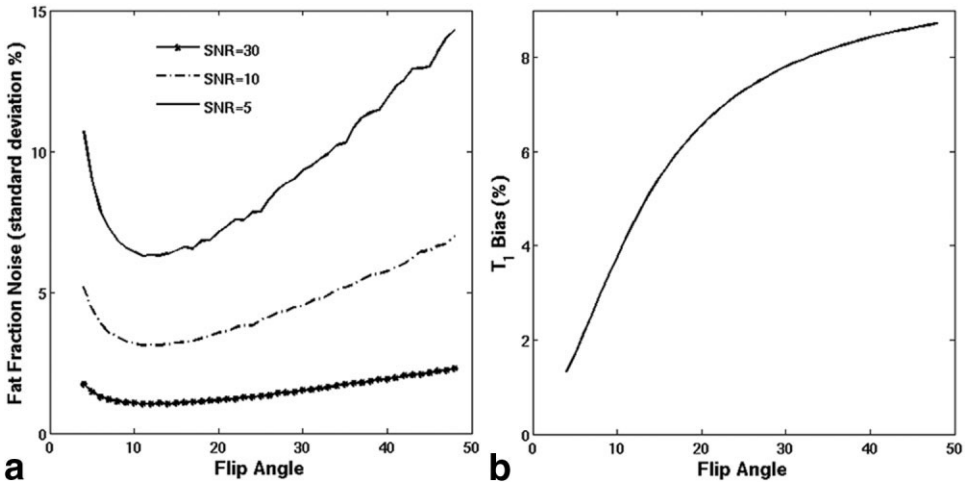

FIG. 3. **a:** Simulated noise (SD) of the fat-fraction estimated after the addition of Gaussian noise added to water and fat signals, using a Monte Carlo simulation (3000 trials for each fat-fraction calculation, with TR = 10 ms, T_{1w} = 586 ms, and T_{1f} = 343 ms) as a function of flip angle, assuming a true fat-fraction of 0.5. The SD of the fat-fraction is plotted as a percentage of the true fat-fraction. The SD of the noise is determined for a given SNR value (= 5, 10, and 30) based on the water signal at its Ernst angle (10.5°, TR = 10 ms, T_{1w} = 586 ms). The minimum noise on the fat-fraction estimate occurs at a flip angle of 12° for all SNR values. The fast rise of the curves below 5° indicates the increasing error in the fat-fraction estimation at low SPGR signal levels. Without consideration of T_1 bias, a flip angle of 12° gives the optimal noise performance in the fat-fraction estimations. **b:** Calculated fat-fraction bias at different flip angles from the same simulation. Bias is the difference in the true fat-fraction (0.5) and the calculated fat signal fraction, which is confounded by the differences in T_1 between water and fat. Bias on fat-fraction bias is independent of image SNR.

(error) that would be introduced into the fat-fraction estimate for various flip angles and overall image SNR levels.

Unlike Fig. 3a, which plots the noise estimate of the fat-fraction, Fig. 3b plots the bias of fat-fraction estimates for at different flip angles from the same simulation. The bias is the difference between the true fat-fraction of 0.5 and the fat signal fraction (calculated using Eq. [2] with confounding T_1 effects). The calculated bias in fat-fraction is independent of SNR, since the bias is simply the difference in true fat-fraction (0.5) and the fat-signal fraction, which is skewed by T_1 effects.

From Fig. 3a, we see that a flip angle of 12° gives optimal SNR performance, with the lowest noise on the fat-fraction estimate for all simulated SNR levels (5–30). This occurs because the overall signal levels from both water and fat are highest near this flip angle, and the overall noise on the calculated fat-fraction is lowest at this flip angle. However, using a 12° flip angle leads to considerable bias (4.5%) as is seen in Fig. 3b. Reducing the flip angle, to 5°, however, offers a good compromise between T_1 bias reduction (the maximum residue bias is 3% for a true fat-fraction of 0.5, i.e., 0.50 ± 0.015) and reasonable SNR performance in the fat-fraction measurement. We refer to this method as the "small flip angle approach."

Dual Flip Angle Method

Despite the effectiveness of the small flip angle approach to reduce the T_1 bias, the low SNR of the small flip angle method raise some concerns for the noise performance of the resulting fat-fraction image. In addition, we wish to find a definitive approach to completely remove T_1 bias, which the small flip angle method cannot achieve. Inspired by the "DESPOT" (Driven-equilibrium single-pulse observation of T_1) techniques described by Deoni et al. (35) for rapid estimation of T_1 maps, we propose a second approach by performing two consecutive imaging acquisitions at two different flip angles, which is referred to as the "dual flip angle" method.

IDEAL-SPGR imaging is performed at two different flip angles, followed by reconstruction into separated fat and water images. With the measured signal amplitudes (S_{1w}, S_{2w} for water and S_{1f}, S_{2f} for fat) and flip angles (α_1, α_2), Eqs. [4] and [5] can be rewritten as Eqs. [9] and [10], to give T_1-corrected water (fat) signal, and therefore η.

$$M_W = \frac{S_{1w}(1 - e^{-TR/T_{1w}}\cos\alpha_1)}{(1 - e^{-TR/T_{1w}})\sin\alpha_1}, \quad \text{where } e^{-TR/T_{1w}} = \frac{S_{1w}\sin\alpha_2 - S_{2w}\sin\alpha_1}{S_{1w}\sin\alpha_2\cos\alpha_1 - S_{2w}\sin\alpha_1\cos\alpha_2} \quad [9]$$

$$M_f = \frac{S_{1f}(1 - e^{-TR/T_{1f}}\cos\alpha_1)}{(1 - e^{-TR/T_{1f}})\sin\alpha_1}, \quad \text{where } e^{-TR/T_{1f}} = \frac{S_{1f}\sin\alpha_2 - S_{2f}\sin\alpha_1}{S_{1f}\sin\alpha_2\cos\alpha_1 - S_{2f}\sin\alpha_1\cos\alpha_2}. \quad [10]$$

An analytical solution for choosing the optimum flip angles was described by Deoni et al. (35), where an optimal flip angle pair that provides the best possible noise performance based on a single value of T_1 can be determined. Using Deoni's approach and assuming T_{1w} = 586 ms and T_{1f} = 343 ms, the two flip angles are 4.4° and 25.0° for water, and 5.8° and 32.3° for fat. This results in different optimal flip angle pairs because of unequal T_1 values. As a preliminary approach, averaged values of 5° and 29° will be used as a pair. Further optimization of flip angles will be thoroughly considered in future work.

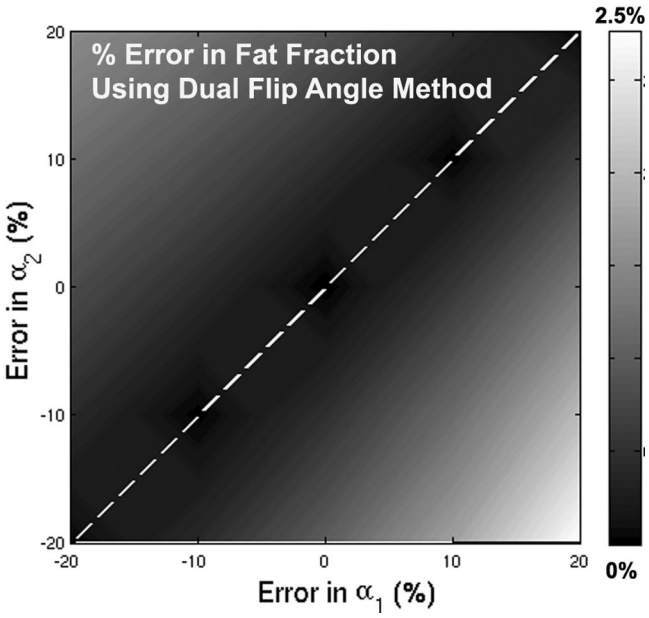

FIG. 4. Effects of B_1 inhomogeneities on dual flip angle T_1 correction methods. Contour plots of the simulated error (percentage of the true fat-fraction, 0.5 for this simulation) in fat-fraction using the dual flip angle method under the influence of B_1 inhomogeneities. Less than a 2.5% error over a wide range of B_1 variation is predicted. If we assume that the relative error in the flip angle is the same for α_1 and α_2 (dashed line), the errors in the estimation of water and fat exactly compensate for one another and there is no error in the estimation of fat-fraction, even with large B_1 inhomogeneities.

A known limitation of DESPOT is its sensitivity to RF (B_1) inhomogeneities, which cause inaccuracy in the expected flip angles and leads to errors in the estimation of proton densities and T_1. However, the fat-fraction will be insensitive to B_1 variation. Figure 4 illustrates the contour plots of the resulting error (percentage of the true fat-fraction, 0.5) for fat quantification in the presence of B_1 inhomogeneities. Less than a 2.5% error over a wide range of B_1 variation is demonstrated. This is due to the fact that errors in the estimation of water and fat compensate for one another, particularly if we assume that relative errors of the flip angles are the same. Since the flip angle is proportional to the B_1 amplitude, there will be almost no error in the estimation of fat-fraction if the relative B_1 error is the same at each flip angle (a reasonable assumption), as indicated by the dashed line in Fig. 4.

Although the dual flip angle method is an attractive approach in the case of unknown T_1, a major restriction of this algorithm is the impact of the noise. If either of separated water or fat signals is low (e.g., true fat-fraction = 0), the estimation of the true water and fat signals (Eqs. [9], [10]) become highly erratic. This occurs because the fat (water) signal in the images acquired at the two flip angles is extremely low and only contains noise. Mathematically, this could arise from a very long, nonphysiological T_1, or from a very low fat (water) signal (which is actually the case); it is difficult to resolve the two scenarios mathematically. In the presence of noise, the calculation of T_1 corrected fat (water) signal using Eqs. [9] and [10] becomes highly unstable. Figure 5a illustrates this effect in a Monte Carlo simulation (3000 trials, SNR = 10), where estimates of fat-fraction becomes highly erratic at low and high fat-fractions.

In this situation, we must rely on additional information. Specifically, we must *constrain* the possible values of T_1 to those that reflect physiologically possible relaxation parameters. In particular, we require that T_1 must be as follows: 1) real, 2) greater than zero, and 3) less than some physiologic upper bound. In this way, we use a priori information to determine the true fat-fraction for very low (high) fat-fractions. Simulations with these assumptions are shown in Fig. 5b, where T_1 is constrained to be real and in the range of $1 < T_1 < 2000$ ms for both water and fat. T_{1w} and T_{1f} are derived from Eqs. [9] and [10], and compared to the limits. For example, if T_{1w} exceeds the upper bound, 2000 ms is used in Eq. [9] to obtain a corrected value for $e^{-TR/T_{1w}}$, which is then applied to calculate the proton density M_w. The calculation of fat-fraction is considerably more stable with this approach, even with mild T_1 constraints.

The small flip angle approach does not suffer from the instability of the unconstrained dual flip angle method, because it does not require any mathematical transformation (e.g., Eqs. [9] and [10]) to determine the fat-fraction.

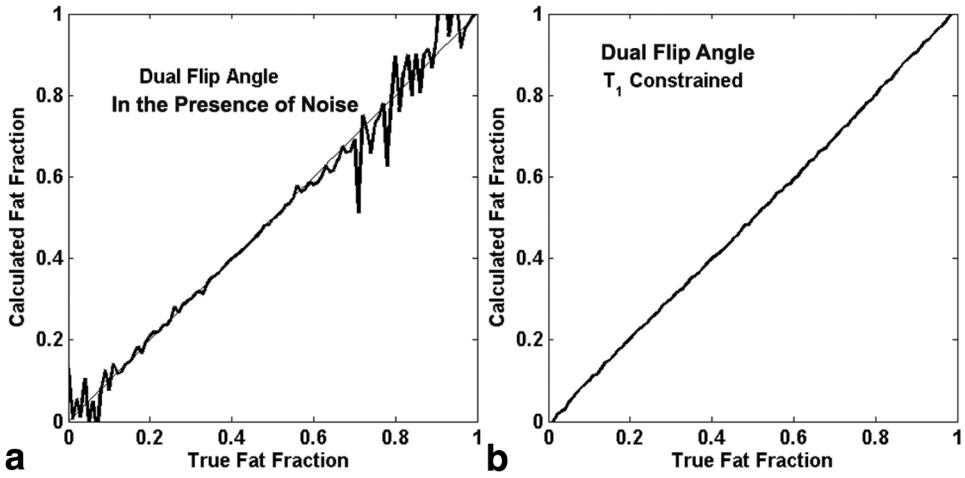

FIG. 5. **a:** Simulated fat-fraction in the presence of noise (SNR = 10), with dual flip angle correction method. Highly erratic estimates of fat-fraction are seen for low and high fat-fraction, due the unstable estimates of T_1. Use of the T_1-constrained method greatly improved estimation of fat-fraction (**b**).

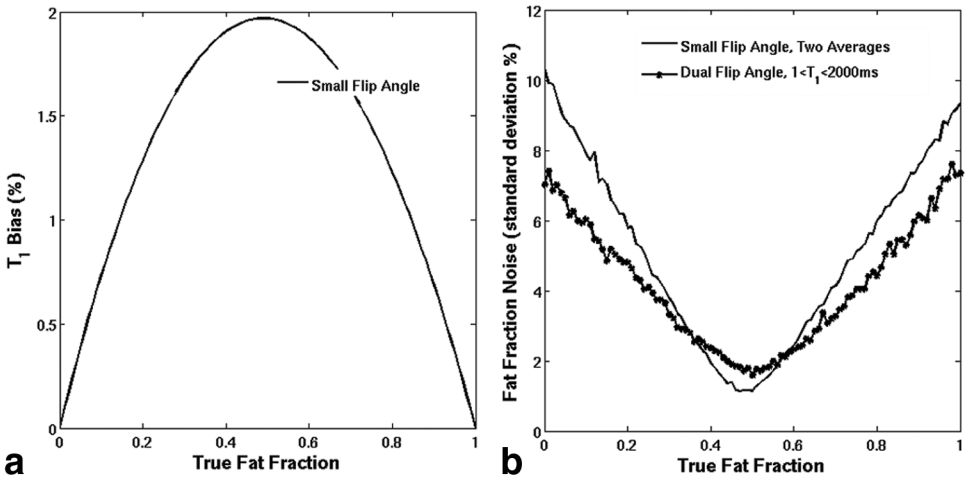

FIG. 6. **a:** Absolute difference between the calculated and true fat-fractions (T_1 bias) using 5° flip angle. The bias for the dual flip angle method is zero. **b:** Noise performance (SD) of the fat-fraction estimation obtained with a Monte Carlo simulation (3000 trials, SNR = 10, with TR = 10 ms, T_{1w} = 586ms, and T_{1f} = 343 ms) using both 5° flip angle with two averages and dual flip angle methods with T_1 constraint limits of $1 < T_1 < 2000$ ms.

As shown in Fig. 3a, the noise performance of the small angle approach does suffer at very small flip angles, however, the calculation of fat-fraction with the small flip angle method is inherently stable, since there is no ambiguity: the low fat (water) signal arises because there is simply little fat (water) in that voxel, reflecting the physics of the SPGR acquisition. The major disadvantage of the small flip angle method compared to the dual flip angle method is the residual bias (Fig. 3b).

In comparison to the small flip angle method, the dual flip angle approach eliminates T_1 bias. Figure 6a plots the absolute difference between the calculated and true fat-fractions (T_1 bias) using a 5° flip angle. The bias for dual flip angle method is zero because the dual flip angle method is an exact analytical solution. Figure 6b plots a Monte Carlo simulation of the noise performance (SD) of the estimated fat-fraction (3000 trials, with TR = 10 ms, T_{1w} = 586 ms, and T_{1f} = 343 ms) using both the small flip angle (5°) with two averages and the dual flip angle method with T_1 constraint. The scan time was the same for both methods in order to compare SNR performance, although it is important to note that the minimum possible scan time for the small flip angle is half that of the dual flip angle method. As for the simulations in Fig. 3a, the noise variance for the simulations in Fig. 6b is based on an SNR value of 10 for water at its Ernst angle (TR = 10 ms, T_1 = 586 ms). The noise performance of the small flip angle method for the same scan time is very similar, or slightly inferior to the dual flip angle method using mild T_1 constraints ($1 < T_1 < 2000$ ms).

Bias Created by Image Noise

For most clinical anatomical imaging applications, evaluation of fat-fraction is performed using the magnitude-separated water and fat images. The noise in complex MR images is Gaussian with zero mean (36), and after performing the magnitude operation, areas with high signal will have unaffected noise statistics. However, in regions of low signal, the noise distribution becomes skewed (Rician) and has a biased, nonzero mean (37). Figure 7a and b compare the noise level when complex and magnitude images are displayed. The signal intensities of the decomposed fat images with low fat content and water images with low water content will be artifactually increased by the noise. Hence, a bias in the fat-fraction with very low and very high fat content regions would be introduced. This effect is demonstrated with a simulation in Fig. 7c, where complex zero-mean Gaussian noise was added to signals (SNR = 10, ignoring T_1 effects). In this example, the magnitude operation makes the noise nonzero mean, causing a positive bias of nearly 8% for very low fat-fractions. This effect would be clinically significant for low fat-fractions and could lead to false-positive diagnoses of mild steatosis.

This bias can also be understood from the definition of fat-fraction. In general, S_w and S_f in Eqs. [4] and [5] are complex and have a different phase. The fat-fraction based on Eq. [2] can be rewritten explicitly with the water and fat signals at different initial phase ϕ_w and ϕ_f, respectively,

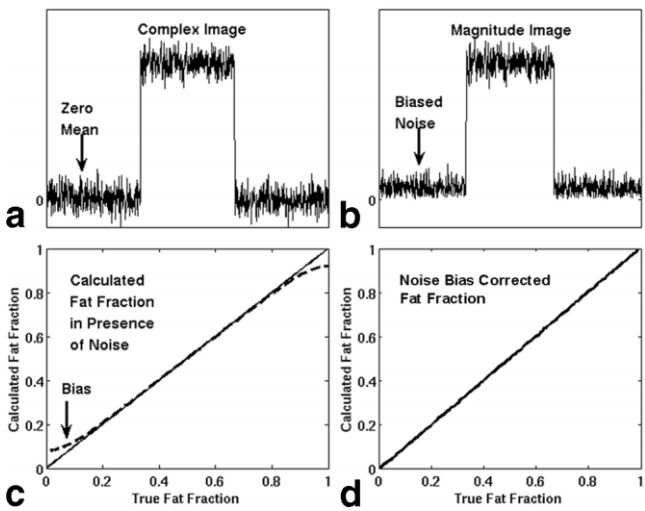

FIG. 7. Noise behavior using SNR = 10 and 3000 trials in a Monte Carlo simulation. Regions of low signal in complex images (**a**) have Gaussian, zero-mean noise. In magnitude images, however, these regions have skewed noise distributions with nonzero, biased noise (**b**), which will lead to biased estimates of low fat-fractions (**c**). Noise bias corrected reconstruction using either the magnitude discrimination or phase-constrained method removes this bias (**d**).

$$\eta_s = \frac{S_f e^{i\varphi_f}}{(S_w e^{i\varphi_w} + S_f e^{i\varphi_f})}. \quad [11]$$

However, if $\phi_w \neq \phi_f$ and both are unknown, the magnitude estimates must be used, i.e.,

$$\eta_s' = \frac{|S_f e^{i\varphi_f}|}{(|S_w e^{i\varphi_w}| + |S_f e^{i\varphi_f}|)} = \frac{|S_f|}{(|S_w| + |S_f|)} \quad [12]$$

When the fat or water signal is low, this leads to a significant bias in η_s' because the nonzero averaged noise exaggerates the signal amplitude. Such bias has been reported by Hussain et al. (19) (Fig. 4), where 5% overestimation of the apparent fat content in pure water was observed in their phantom studies. We believe that the noise-related effect described above may be the source of this bias.

We first propose a "magnitude discrimination" method to eliminate the noise bias. This method applies if we can assume that the signal from fat and/or water is sufficiently high that noise remains zero-mean. The first step is to estimate water and fat with the conventional IDEAL algorithm. Next, the IDEAL signal model is modified slightly to estimate the sum of fat and water signals,

$$\begin{aligned} s(t_n) &= (S_w + S_w e^{i2\pi\Delta f t_n}) e^{i2\pi\psi t_n} \quad [13] \\ &= (S_w + (S_w + S_f - S_w) e^{i2\pi\Delta f t_n}) e^{i2\pi\psi t_n} \\ &= (S_w \cdot (1 - e^{i2\pi\Delta f t_n}) + (S_w + S_f) \cdot e^{i2\pi\Delta f t_n}) e^{i2\pi\psi t_n}, \end{aligned}$$

where t_n is echo time, Δf is the chemical shift frequency, and ψ is the local field inhomogeneity. Estimation of $|S_w + S_f|$ provides an estimate of the denominator without noise bias. Next, the signals from water and fat are compared to determine which is the dominant component (i.e., water is dominant if $S_w > S_f$, and vice versa). If fat is the dominant component, the fat-fraction is calculated as $\eta_s = |S_f|/|S_f + S_w|$; otherwise, $\eta_s = 1 - (|S_w|/|S_f + S_w|)$ if water dominates. Here we have exploited the fact that the sum of the fat-fraction ($S_f/(S_f + S_w)$) and the "water fraction" ($S_w/(S_f + S_w)$) must equal 1. By choosing the larger component, we avoid noise bias in the numerator. It is worth noting that any method that acquires an in-phase image (14,15), the magnitude in-phase image will have no noise bias and can be used as the denominator of the fat-fraction calculation. However, the magnitude discrimination for the numerator must be performed in the same way.

However, if low SNR exists in both fat and water images, a "phase-constrained" method can be used. A phase-constrained approach has been implemented by Yu et al. (38) as part of a one-point water-fat separation method for dynamic contrast enhanced imaging. This method assumes that the phase of water and fat within a voxel are equal at TE = 0. This is a very reasonable assumption, which directly reflects the physics of SPGR pulse sequences, where the phases of water and fat are equal at TE = 0. In fact, most other water-fat separation methods (12–15) make this assumption, i.e., $\phi_w = \phi_f \equiv \phi$. Unlike these methods, IDEAL does not require that the phase of water and fat be equal at TE = 0, which provides increased flexibility for other pulse sequences such as balanced steady state free precession (SSFP). This flexibility is not required for SPGR imaging, however. Using this assumption, Eq. [11] becomes,

$$\eta_s = \frac{S_f e^{i\varphi}}{(S_w e^{i\varphi} + S_f e^{i\varphi})} = \frac{S_f}{S_w + S_f}. \quad [14]$$

The decomposed fat/water images are real quantities (not complex) and the resulting fat-fraction will have nonbiased zero-mean noise. Using this model, we avoid taking the magnitude of a complex signal to estimate the fat-fraction. Figure 7d shows the reduced bias from the image noise using both approaches.

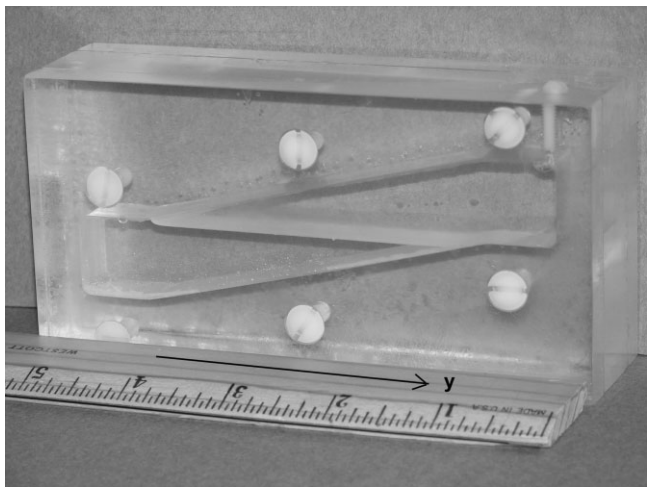

FIG. 8. Photograph (axial view) of the fat/water phantom with oil floating on top of water in the Plexiglas cavity. The arrow (y) denotes the long axis of the phantom. This configuration provides a true volume fat-fraction ranging linearly from 0% to 100%.

MATERIALS AND METHODS

A phantom designed to create a continuum of fat-fractions was constructed as shown in Fig. 8. This phantom consisted of two trapezoids filled with equal volumes of olive oil and water doped with $CuSO_4$ (2.3 mM/liter). The oil-water interface of the trapezoids is shifted to each side to create a 100% water region, linearly varying oil/water ratio region, and a 100% oil region. To reduce surface tension and create a flat, smooth interface between water and fat, a small amount (~0.5 ml) of surfactant (Merpol A surfactant; Sigma-Aldrich, St. Louis, MO, USA) was added to the water. Without the surfactant, a significant meniscus occurred between the acrylic, water, and oil interface because of the phantom geometry and different water-oil surface tension.

Experiments were performed on 1.5T clinical scanners (TwinSpeed EXCITE; GE Healthcare, Waukesha, WI, USA) using a transmit-receive single channel quadrature head coil for most of the studies. To measure the bias due to image noise, low SNR data were collected using the body coil.

Phantom Calibration

We measured the T_1 values of the oil and water in the phantom to validate the T_1 correction algorithm and calculate the two flip angles used in the dual flip angle method. In general, T_1 mapping is not considered as routine process in vivo for fat quantification, however, we wished to characterize our phantom. T_1 measurements were carried out using an inversion-recovery fast spin echo (IR-FSE) sequence with a variable inversion time (TI) and T_2 values were determined using a spin echo (SE) sequence at various TEs. Axial images from the lateral view of the phantom (shown in Fig. 7) were acquired.

To spatially register the percentage of oil along the long axis of the phantom, we performed a calibration scan using a 2D IDEAL-SPGR sequence prescribed in the axial plane as described in the T_1 measurements. Imaging parameters included TR = 11.3 ms, TE = 4.4, 6.0, and 7.5 ms, corresponding to optimized IDEAL echo shifts at 1.5T (16), slice = 50 mm, FOV = 14 cm, Nx = Ny = 256, bandwidth (BW) = ± 31.25 kHz, and $\alpha = 45°$. A continuum of fat-fractions was linearly scaled between 0% and 100%. This fat-fraction was based on an assumption of equivalent fat and water proton densities at each position and could be considered as volume fat-fraction. Throughout the following sections, this was also named "true fat-fraction" for simplification.

Calibration was necessary to account for slight imperfections (meniscus) in the phantom. Differences in proton density were removed as part of this calibration, in order to determine the true fat-fraction for comparison. Removal of proton density differences does not complicate the T_1 and noise bias compensation methods and no such calibrations will be necessary for in vivo applications. A single coronal slab parallel to the floor of the phantom was acquired. To avoid chemical shift artifacts, the phase encoding direction was oriented along the long axis of the phantom. Water or fat signal amplitude was calculated at each location along this axis. The protocol presented in the previous study was used with proton density weighting (TR = 4 s, TE = 4.4, 6.0, and 7.5 ms, $\alpha = 90°$). The curve of the resultant fat signal fraction was calibrated with the volume fat-fraction. This permitted the examination of T_1 and noise bias without the complication of proton density differences and minimal residual menisci in the phantom.

T_1 Correction

To examine the flip angle dependence of the fat-fraction, the acquisition scheme presented in the previous calibration study was used and a 2D IDEAL-SPGR sequence (TR = 11.3 ms, TE = 4.4, 6.0, and 7.5 ms) was applied with flip angles ranging from 5° to 45°. Both T_1 bias and the SNR performance were evaluated for decreasing flip angles.

To validate the proposed dual flip angle method, we first calculated two pairs of optimum flip angles from the measured T_1 values for water and fat respectively using Deoni et al.'s (35) approach. Phantom images were acquired using the final averaged two flip angles. Imaging parameters were the same as in the flip angle studies.

Noise Bias Correction

Finally, we investigated the bias created by image noise by performing low SNR measurements using the body coil and the same imaging parameters as the T_1 correction studies. In particular, we used a bottle phantom containing only water to ensure that the fat-fraction was truly zero. Images with six different SNR values were acquired by changing the number of averages (1, 4, 10, 20, 40, and 80) and $\alpha = 5°$ to reduce T_1 bias. Image reconstruction was performed offline using programs written in Matlab (Mathworks, Natick, MA, USA). The fat-fractions calculated with both magnitude discrimination and phase-constrained approaches were compared to those estimated using the regular magnitude data method.

RESULTS

T_1 and T_2 values obtained from the phantom at 1.5T were 628 ± 8 ms and 520 ± 10 ms for water, and 175 ± 3 ms and 90 ± 10 ms for fat, respectively. The measured T_2 values were relatively long compared to the TE used in the imaging protocol of SPGR sequence for fat quantification. Hence, T_2* effects were ignored.

Examples of the 2D IDEAL-SPGR fat-water separated images are shown in Fig. 9. The axial images (Fig. 9a and b) provided the reference for pixel location and its corresponding true fat-fraction. The coronal slab images (Fig. 9c and d), which covered a continuous transition from mostly water pixels to mostly oil pixels, were used in the fat signal fraction calculations as described in the MRI algorithm.

In Fig. 10a, the behavior of the fat signal fractions (calculated oil content) agrees well with the simulation (Fig. 1b), and demonstrates the utility of the small flip angle method, in which fat-fraction bias is reduced as flip angle is decreased. A maximum error of 40.5% was observed with $\alpha = 30°$ data and 7.5% error with $\alpha = 5°$ data assuming a true fat-fraction of 0.5 (Fig. 10b). Although the small flip angle results correlated well with true values, the SNR of the fat image acquired with $\alpha = 5°$ was 38.5% lower than that acquired with $\alpha = 30°$ (Fig. 10c). SNR was evaluated with signals drawn from pure oil and pure water regions in the separated fat and water images. Because of its long T_1 value, water SNR was lower than that of fat as predicted in Fig. 1a.

To validate the dual flip angle method in fat quantification, we first calculated the optimum flip angles according to the analytic solution given by Deoni et al. (35) using T_1 values of water and fat measured in the phantom. flip angles of 4° and 24° were derived theoretically for water,

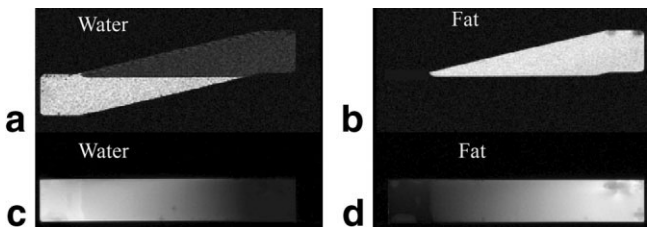

FIG. 9. 2D IDEAL-SPGR fat-water separated images. **a**,**b:** Axial images through the phantom. These images provided reference for pixel location and its corresponding true fat-fraction. **c**,**d:** Coronal slab images that consisted of a continuous transition from pure water (left side of image) to pure oil (right side of image).

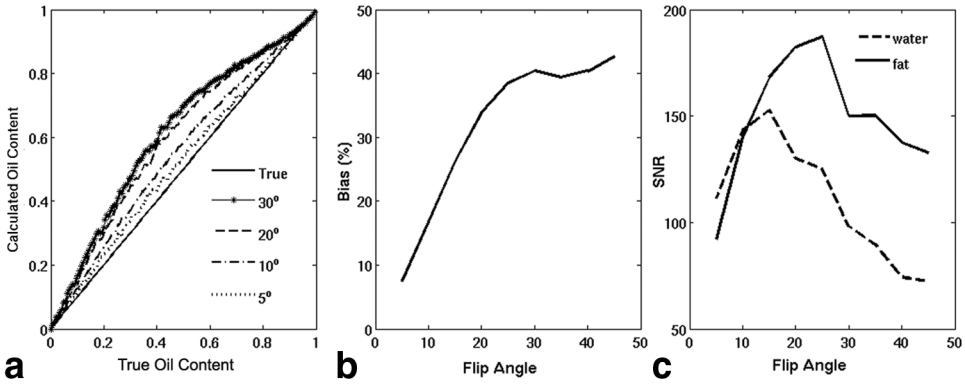

FIG. 10. **a:** Calculated oil content measured at different flip angles, which agree with the confounding T_1 effects predicted by theory. **b:** Bias of fat signal fractions vs. flip angles. Results were calculated from (a) at a fat-fraction of 0.5. **c:** SNR performance of fat and water at different flip angles. Signals were measured from pure water and pure oil regions. Because of its longer T_1 value, water SNR was lower than that of fat. These measurements were consistent with the simulations shown in Fig. 1, and provide experimental confirmation of the small flip angle approach for reducing T_1-related bias.

with 8° and 44° for fat. Hence, we used the averaged values 6° and 34° as a pair of flip angles for both water and fat images. Figure 11a demonstrates the feasibility of this approach. The estimated fat-fraction agrees well with the expected values, indicating the effectiveness of this method. Improved estimation of fat-fraction was seen after T_1-constrained (Fig. 11b). For this phantom studies, T_1 was constrained to be real, and in the range of $1 < T_1 < 2000$ ms for both water and fat to avoid erroneous values of T_1 as indicated by the spikes at 15% and 95% fat-fractions. Figure 11b and the 5° curve in Fig. 10a also allow quantitative performance comparison between the two techniques for T_1 correction. The mean absolute differences between the calculated and true fat-fractions are 1.9% and 3.0% for the dual flip angle and small flip angle method, respectively. Depending on the severity of steatosis, theses results provide references for choice of the techniques for quantification of hepatic fat content with considerations including the SNR, scan time, and T_1 bias.

Figure 12 shows in vitro results of the bias created by image noise in fat quantification acquired using the body coil, plotted against the SNR of the water images. The bias is the difference between the calculated fat-fraction and its true value, which is zero in the water phantom. The skewed, nonzero mean image noise resulted in a 4% to 15% bias in calculated fat-fraction when using the most obvious approach (magnitude data). This bias was reduced to below 1% using either magnitude discrimination or phase-constrained IDEAL.

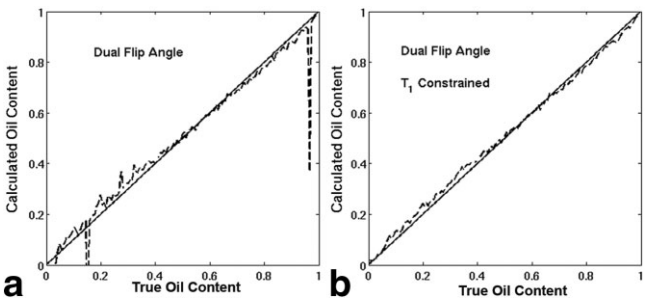

FIG. 11. Fat-fraction estimated with dual flip angle correction method. **a:** The estimated fat-fraction agrees well with the expected values. **b:** Improved estimation, without spurious fat-fractions are achieved using the T_1-constrained approach.

DISCUSSION

A highly accurate means of quantifying hepatic steatosis would be extremely beneficial for the diagnosis, treatment, and early intervention of NAFLD, as well as for clinical trials developing new treatments for NAFLD. Although MRI is capable of separating water signal from fat, the quantitative measurement of the fat content of the liver

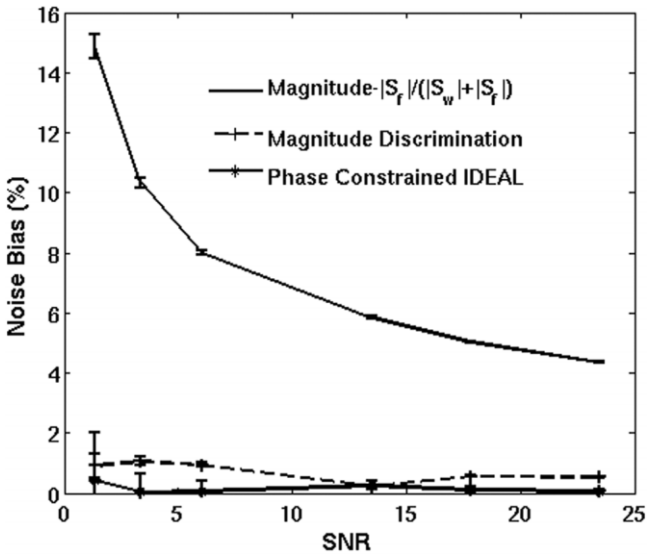

FIG. 12. Bias created by image noise in fat quantification measured in the water-only phantom, plotted as a function of the SNR of the water images. The skewed, nonzero mean image noise resulted in a 4% to 15% bias in calculated fat-fraction when using the most obvious approach (magnitude data). This bias was reduced to below 1% using either magnitude discrimination or phase-constrained IDEAL.

using MRI is technically challenging. True fat quantification should be independent of imaging sequences and protocols. However, naive calculation of the signal fraction will be confounded by the effects of T_1 and T_2*, with potentially large, pulse sequence–dependent bias. To accurately quantify the fat-fraction with rapid volumetric gradient echo methods, two dominant sources of bias should be addressed: differences in water and fat relaxation times, and image noise. We have demonstrated the feasibility of small angle and dual-flip angle approaches to reduce T_1 effects. By using magnitude discrimination or phase-constrained methods, true fat-fraction can be estimated without noise bias.

The effects of T_2* are negligible in normal livers, and are generally ignored for short-TE gradient echo imaging. In the presence of iron deposition, however, T_2* is shortened due to increased signal dephasing. The signal decays more rapidly, corrupting the water-fat decomposition and disrupting the calculation of true fat-fraction. The relationship between iron content and measurements of T_2* using the T_2*-corrected IDEAL method (21) will be explored in future studies, and is beyond the scope of this work. Furthermore, both the T_1 and noise bias corrections described in this study can be incorporated into the T_2*-corrected IDEAL to address the clinical utility of this method. This may provide insight into the presence of iron in patients with chronic liver disease and be helpful in the development of noninvasive methods for quantification of hepatic iron overload.

The noise performance of the dual flip angle method was similar, or perhaps slightly improved, compared to the small flip angle method (with $\alpha = 5°$). In addition, the dual flip angle method entirely eliminates bias. Unfortunately, this approach requires the sequential acquisition of two images, which may be challenging for breathhold applications such as liver imaging. For applications in which scan time is a limitation and a small amount of bias may be tolerable, the small flip angle approach may be the preferred method. As an example, consider a true fat-fraction of 0.15. From Fig. 6a, we see that there will be a small bias of approximately 0.8% (i.e., 0.15 ± 0.0012) using the small flip angle method. The dual flip angle method, however, requires twice the minimum scan time compared to the small flip angle approach, but will have an SNR improvement of approximately 24% for this fat-fraction, for the same scan time (Fig. 6b).

Our proposed dual angle method removes the bias from T_1 effects, even though flip angle pairs were not optimized. Although the precise selection of optimized flip angles is not necessary to obtain fat-fraction images free from T_1 bias, the optimal choice of flip angles would improve the noise performance of the fat-fraction estimates. The prior optimization by Deoni et al. (35) cannot be extrapolated because of the estimation of a range of T_1 values. The noise performance of fat-fraction estimation should be investigated through calculation of the Cramér-Rao bound (CRB) (39) to determine the optimal choice of flip angles. The CRB represents the theoretically best noise performance that can be achieved by a signal estimation method; any estimator that matches the CRB is said to be "efficient." The optimal choice of flip angles will be computed as a weighted average across the variances over the range of biologically reasonable T_1 values for water and fat. The CRB will help predict the best possible combination of flip angles that optimizes the noise performance of the fat-fraction estimation. When using the dual flip angle approach, it is important to constrain T_1 to reasonable values in order to avoid erroneous estimates of fat-fraction.

Although the small flip angle approach is simpler and does not require special image reconstruction, there is a residual flip angle-dependent T_1 bias introduced into the estimated fat-fraction (Fig. 6a). However, the noise performance of the small flip angle approach is similar to the dual flip angle method when using the same total scan time (Fig. 6b), even with considerable T_1 constraint. Further improvement in the noise performance of the dual flip angle method will be possible with optimization of the flip angles for this approach, as well as through refinement of T_1 constraint methods. The major disadvantage of the dual flip angle method is the doubling of scan time, which may be alleviated through the use of phased array coils and parallel imaging (25). The choice of T_1 correction method will likely depend on the specific application: applications that are scan time limited but can tolerate a small amount of residual bias may prefer the small flip angle method. Conversely, applications that are not limited by scan time may prefer the dual flip angle method to achieve the lowest possible T_1 bias.

CONCLUSIONS

We have validated the IDEAL-SPGR method for quantification of fat-fraction in a phantom, reducing or removing the effects of T_1 bias, and removing the effects of noise bias. Small-flip angle or dual-flip angle approaches are two alternatives to minimize the T_1 bias. Magnitude discrimination and phase-constrained methods can effectively remove noise bias. Finally, clinical validation will be needed for complete validation of this method for the accurate quantification of hepatic steatosis.

ACKNOWLEDGEMENTS

We thank Ernest Madsen and Gary Frank for their assistance in the oil/water phantom construction. SBR is the recipient of an Afga Laboratories Radiological Society of North America Research Scholar Grant.

REFERENCES

1. Wanless IR, Lentz JS. Fatty liver hepatitis (steatohepatitis) and obesity: an autopsy study with analysis of risk factors. Hepatology 1990;12: 1106–1110.
2. Harrison SA, Neuschwander-Tetri BA. Nonalcoholic fatty liver disease and nonalcoholic steatohepatitis. Clin Liver Dis 2004;8:861–879, ix.
3. Marchesini G, Brizi M, Bianchi G, Tomassetti S, Bugianesi E, Lenzi M, McCullough AJ, Natale S, Forlani G, Melchionda N. Nonalcoholic fatty liver disease: a feature of the metabolic syndrome. Diabetes 2001;50: 1844–1850.
4. Brunt EM. Pathology of nonalcoholic steatohepatitis. Hepatol Res 2005.
5. Chitturi S, Abeygunasekera S, Farrell GC, Holmes-Walker J, Hui JM, Fung C, Karim R, Lin R, Samarasinghe D, Liddle C, Weltman M, George J. NASH and insulin resistance: Insulin hypersecretion and specific association with the insulin resistance syndrome. Hepatology 2002;35: 373–379.
6. Chitturi S, Farrell GC. Etiopathogenesis of nonalcoholic steatohepatitis. Semin Liver Dis 2001;21:27–41.

7. Brunt EM. Nonalcoholic steatohepatitis. Semin Liver Dis 2004;24:3–20.
8. Ratziu V, Charlotte F, Heurtier A, Gombert S, Giral P, Bruckert E, Grimaldi A, Capron F, Poynard T. Sampling variability of liver biopsy in nonalcoholic fatty liver disease. Gastroenterology 2005;128:1898–1906.
9. Bravo A, Sheth S, Chopra S. Liver biopsy. N Engl J Med 2001;344:495–500.
10. Lin HZ, Yang SQ, Chuckaree C, Kuhajda F, Ronnet G, Diehl AM. Metformin reverses fatty liver disease in obese, leptin-deficient mice. Nat Med 2000;6:998–1003.
11. Bugianesi E, Gentilcore E, Manini R, Natale S, Vanni E, Villanova N, David E, Rizzetto M, Marchesini G. A randomized controlled trial of metformin versus vitamin E or prescriptive diet in nonalcoholic fatty liver disease. Am J Gastroenterol 2005;100:1082–1090.
12. Dixon WT. Simple proton spectroscopic imaging. Radiology 1984;153:189–194.
13. Glover G. Multipoint Dixon technique for water and fat proton and susceptibility imaging. J Magn Reson Imaging 1991;1:521–530.
14. Xiang Q, An L. Water-fat imaging with direct phase encoding. J Magn Reson Imaging 1997;7:1002–1015.
15. Ma J. Breath-hold water and fat imaging using a dual-echo two-point Dixon technique with an efficient and robust phase-correction algorithm. Magn Reson Med 2004;52:415–419.
16. Reeder SB, Wen Z, Yu H, Pineda AR, Gold GE, Markl M, Pelc NJ. Multicoil Dixon chemical species separation with an iterative least-squares estimation method. Magn Reson Med 2004;51:35–45.
17. Martin J, Sentis M, Puig J, Rue M, Falco J, Donoso L, Zidan A. Comparison of in-phase and opposed-phase GRE and conventional SE MR pulse sequences in T1-weighted imaging of liver lesions. J Comput Assist Tomogr 1996;20:890–897.
18. Siegelman ES, Rosen MA. Imaging of hepatic steatosis. Semin Liver Dis 2001;21:71–80.
19. Hussain HK, Chenevert TL, Londy FJ, Gulani V, Swanson SD, McKenna BJ, Appelman HD, Adusumilli S, Greenson JK, Conjeevaram HS. Hepatic fat fraction: MR imaging for quantitative measurement and display—early experience. Radiology 2005;237:1048–1055.
20. de Bazelaire CM, Duhamel GD, Rofsky NM, Alsop DC. MR imaging relaxation times of abdominal and pelvic tissues measured in vivo at 3.0 T: preliminary results. Radiology 2004;230:652–659.
21. Yu H, McKenzie CA, Shimakawa A, Pelc NJ, Brittain JH, Reeder SB. IDEAL Water-fat separation with simultaneous T2* estimation. In: Proceedings of the 14th Annual Meeting of ISMRM, Seattle, WA, USA, 2006 (Abstract 624).
22. Reeder SB, Pineda AR, Wen Z, Shimakawa A, Yu H, Brittain JH, Gold GE, Beaulieu CH, Pelc NJ. Iterative decomposition of water and fat with echo asymmetry and least-squares estimation (IDEAL): application with fast spin-echo imaging. Magn Reson Med 2005;54:636–644.
23. Reeder S, Pineda A, Yu H, et al. Water-fat separation with IDEAL-SPGR. In: Proceedings of the 13th Annual Meeting of ISMRM, Miami Beach, FL, USA, 2005 (Abstract 105).
24. Pineda AR, Reeder SB, Wen Z, Pelc NJ. Cramer-Rao bounds for three-point decomposition of water and fat. Magn Reson Med 2005;54:625–635.
25. McKenzie C, Reeder S, Shimakawa A, Pelc N, Brittain J. Abdominal three point Dixon imaging with self calibrating parallel MRI. In: Proceedings of the 12th Annual Meeting of ISMRM, Kyoto, Japan, 2004 (Abstract 917).
26. Reeder S, Vu AT, Hargreaves BA, Shimakawa A, Wieben O, McKenzie CA, Polzin JA, Brittain JH. Rapid 3D-SPGR imaging of the liver with multi-echo IDEAL. In: Proceedings of the 14th Annual Meeting of ISMRM, Seattle, WA, USA, 2006 (Abstract 2444).
27. Schonfeld G, Patterson BW, Yablonskiy DA, Tanoli TS, Averna M, Elias N, Yue P, Ackerman J. Fatty liver in familial hypobetalipoproteinemia: triglyceride assembly into VLDL particles is affected by the extent of hepatic steatosis. J Lipid Res 2003;44:470–478.
28. Brix G, Heiland S, Bellemann M, Koch T, Lorenz W. MR imaging of fat-containing tissues: valuation of two quantitative imaging techniques in comparison with localized proton spectroscopy. Magn Reson Imaging 1993;11:977–991.
29. Yeung DKW, Griffith JF, Antonio GE, Lee FKH, Woo J, Leung PC. Osteoporosis is associated with increased marrow fat content and decreased marrow fat unsaturation: a proton MR spectroscopy study. J Magn Reson Imaging 2005;22:279–285.
30. Fram EK, Herfkens RJ, Johnson GA, Glover GH, Karis JP, Shimakawa A, Perkins TG, Pelc NJ. Rapid calculation of T1 using variable flip angle gradient refocussed imaging. Magn Reson Imaging 1987;5:201.
31. Bydder M, Middleton MS, Chavez AD, Sirlin CB. Effect of flip angle on fat quantification by Dixon techniques. In: Proceedings of the 14th Annual Meeting of ISMRM, Seattle, WA, USA, 2006 (Abstract 2300).
32. Westwood M, Anderson LJ, Firmin DN, Gatehouse PD, Charrier CC, Wonke B, Pennell DJ. A single breath-hold multiecho T2* cardiovascular magnetic resonance technique for diagnosis of myocardial iron overload. J Magn Reson Imaging 2003;18:33–39.
33. George DK, Goldwurm S, MacDonald GA, Cowley LL, Walker NI, Ward PJ, Jazwinska EC, Powell LW. Increased hepatic iron concentration in nonalcoholic steatohepatitis is associated with increased fibrosis. Gastroenterology 1998;114:311–318.
34. Das SK, Ray K. Wilson's disease: an update. Nat Clin Pract Neurol 2006;2:482–493.
35. Deoni SC, Rutt BK, Peters TM. Rapid combined T_1 and T_2 mapping using gradient recalled acquisition in the steady state. Magn Reson Med 2003;49:515–526.
36. McVeigh ER, Henkelman RM, Bronskill MJ. Noise and filtration in magnetic resonance imaging. Med Phys 1985;12:586–591.
37. Henkelman RM. Measurement of signal intensities in the presence of noise in MR images. Med Phys 1985;12:232–233.
38. Yu H, Reeder SB, McKenzie CA, Brau, ACS, Shimakawa A, Brittain JH, Pelc NJ. Single acquisition water-fat separation: feasibility study for dynamic imaging. Magn Reson Med 2005;55:413–422.
39. Barrett HH, Myers KJ. Foundations of image science. New York: Wiley; 2004.